Existence of in-Plane Magnetic Skyrmion and its Motion under Current Flow

Kyoung-Woong Moon, Jungbum Yoon, Changsoo Kim, and Chanyong Hwang*
Spin Convergence Team, Korea Research Institute of Standards and Science, Daejeon 34113, Republic of Korea

(Received 28 May 2019; revised manuscript received 13 October 2019; published 24 December 2019)

A magnetic skyrmion usually refers to a twisted spin texture in a uniformly aligned magnetization state. Such spin texture is protected by topology, which makes the skyrmion a stable texture under small perturbations. Thus, skyrmions have attracted great interest for possible applications as an ideal information carrier. Most magnetic skyrmion studies have focused on perpendicularly magnetized systems, where the skyrmion topological charge is determined by the relative orientation between the core and outer perpendicular magnetization directions. Thus, skyrmions with opposite signs of topological charges do not seem to coexist in the same magnetic domain. Here we show that there also exists a different type of magnetic skyrmion with surrounding spins that are uniformly aligned to the in-plane direction. A clear feature of this in-plane skyrmion is that skyrmions with opposite signs of topological charges can coexist with each other. Proper choice of magnetization and Dzyaloshinskii-Moriya interaction leads to a window for the existence of this in-plane skyrmion. These findings demonstrate the inherent possibility of a double-bit transfer in a single magnetic wire, which is not possible in a perpendicularly magnetized system.

DOI: 10.1103/PhysRevApplied.12.064054

I. INTRODUCTION

Magnetization is a vector quantity having a direction. If the direction of the magnetization is distinguishable, magnetization with two different directions can be used to form a data bit. A well-known example is a hard-disk drive, which stores information as up and down magnetizations on a rotating disk. Magnetic random-access memory is another example, where many independent magnetic cells containing individual magnetization directions constitute the memory [1,2]. All of these devices are based on a situation in which each magnetization is localized in each position. Thus, data processing requires a rotating disk (for a hard-disk drive) or selecting bits (for magnetic random-access memory). In contrast to this, there is other concept based on translation of magnetization textures in continuous materials [3–5]. In this case, the stability of data directly depends on the stability of the magnetic texture. So a magnetic skyrmion has drawn great interest for future applications because the skyrmion is known to be topologically protected [6,7] until a continuum description of magnetization is valid [8]. In this paper, we focus on fundamental properties of the skyrmion to extend our scope of the skyrmion that will show the possibility of doubling the data density for applications.

II. SKYRMIONS IN PERPENDICULAR-MAGNETIC-ANISOTROPY SYSTEMS

It is a common assumption that two-dimensional magnetic skyrmions exist in a system with perpendicular magnetic anisotropy (PMA) [3,4,9–12], which prefers only up or down magnetization directions. The invariance of the topological charge under any continuous transformations of the spin textures [3,4,7,13,14] leads to the robustness of a magnetic skyrmion against external perturbations, making it ideal to use skyrmions as information carriers for memory and logic applications [3,4,11,12]. A skyrmion can be regarded as a topological defect in a uniform perpendicularly magnetized state. Figure 1(a) shows a typical spin state of a skyrmion in uniform magnetization along the $-z$ (down) direction (black arrows). At the center of the skyrmion, there is a core magnetization along the $+z$ (up) direction (white arrows) opposite the outer background magnetization. Between the core and the outer region, there is a domain wall where the magnetization has to rotate in space to connect the up magnetization and the down magnetization. As a result, pure in-plane magnetization is required at the center of the domain wall (rainbow color arrows) that wraps the $+z$ core.

To form the skyrmion state, the warping magnetization should have a rotational symmetry. A sufficient effective magnetic field for holding the magnetization can be generated by the Dzyaloshinskii-Moriya interaction (DMI) [15,16], which generates a DMI field ($\mathbf{H}_{\mathrm{DMI}}$) where the magnetization gradient occurs. In this paper, we basically

*cyhwang@kriss.re.kr

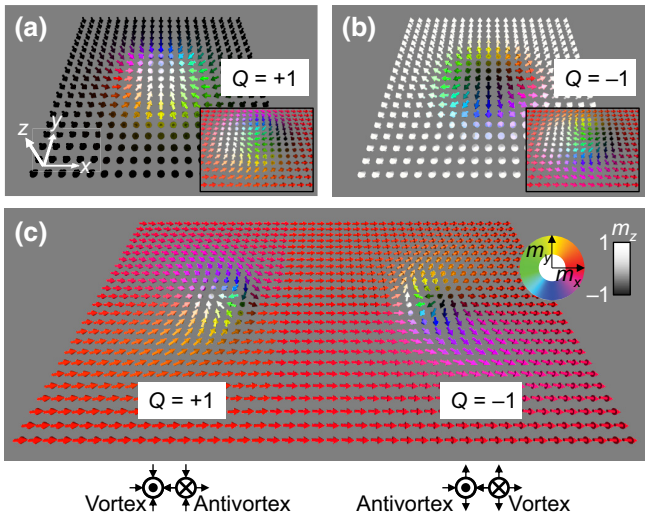

FIG. 1. Skyrmion states in a perpendicular system and in an in-plane system. (a) Skyrmion with $Q = +1$. Arrows represent local magnetization, white and black colors show the z-direction magnetization, and rainbow colors represent magnetization in the x-y plane. The inset shows a rotated magnetization state. (b) Skyrmion with $Q = -1$. (c) Coexistence of skyrmions in an in-plane-magnetization system. The lower panel shows simplified magnetization states. (a), (b) show schematic images and (c) shows a simulation result. The parameters are as follows: exchange stiffness constant $A = 1.3 \times 10^{-11}\,\mathrm{J\,m^{-1}}$, interfacial-DMI energy density $D_{\mathrm{ind}} = 2 \times 10^{-3}\,\mathrm{J\,m^{-2}}$, saturation magnetization $M_S = 720 \times 10^3\,\mathrm{A\,m^{-1}}$, and magnetic layer thickness ($t_M = 1$ nm). The total size is $250 \times 150 \times 1$ nm^3 and the cell sizes are $2 \times 2 \times 1$ nm^3. The magnetic state of the $6 \times 6 \times 1$ nm^3 area is shown as one vector.

assume an interfacial-type DMI (iDMI) [3,17–19] unless specified otherwise; thus, $\mathbf{H}_{\mathrm{DMI}}$ prefers a certain chiral spin texture such as $(-z)$-$(+x)$-$(+z)$-$(-x)$-$(-z)$ along the x axis. If we consider the same chiral spin configuration for the y axis also, we come up with the basic skyrmion texture [Fig. 1(a)]. Figure 1(b) presents the other skyrmion state with the outer magnetization $+z$. In this situation, the core magnetization becomes $-z$ and the warping in-plane magnetization should be reversed to maintain the same chiral spin configuration because of iDMI. Regardless of the core direction, $\mathbf{H}_{\mathrm{DMI}}$ causes the skyrmion to be symmetrically centered at the skyrmion core. Thus, the skyrmion in PMA looks like a circular bubble domain.

Without considering the spin texture at the boundary, this circular domain structure has been claimed to be the skyrmion. However, the exact meaning of "skyrmion" originates from the topology [7,13,20,21]. The topology does not determine the detailed configuration; that is, the size and the shape of an arbitrary magnetic texture cannot be the criterion for claiming a skyrmion. The only criterion is the topological charge, defined as $Q = (1/4\pi) \int \mathbf{m} \cdot (\partial_x \mathbf{m} \times \partial_y \mathbf{m})\, dxdy$, where Q is the skyrmion charge and $\mathbf{m}$ $[(m_x, m_y, m_z)]$ is the normalized magnetization vector at a certain position (x, y). When Q is quantized at the value ± 1, we can refer to this state as a skyrmion. For example, Q is $+1$ for Fig. 1(a) and Q is -1 for Fig. 1(b). From these figures, it seems impossible for skyrmions with opposite Q to coexist in the same outer background magnetization. In detail, the skyrnion in Fig 1(b) cannot exist in the $-z$ domain. However, from the basic nature of the skyrmions, we will see that this is not the case in an in-plane-magnetization system.

III. SKYRMIONS IN IN-PLANE-MAGNETIC-ANISOTROPY SYSTEMS

The skyrmion charge is conserved under continuous transformations such as translation and rotation [17]. Translation is directly related to skyrmion motion [3,4,22]; a position change of a skyrmion does not change the skyrmion charge. This gives us a clue for building the skyrmion in an in-plane-magnetic-anisotropy (IMA) system. We consider a vector rotation by an angle of 90° about the y axis. The inset in Fig. 1(a) shows the result of rotation of the PMA skyrmion ($Q = +1$). The outer magnetization changes from $-z$ to $+x$ and the core magnetization changes from $+z$ to $-x$. After the rotation, the $\pm z$ magnetizations appear at the side of the skyrmion. Similar vector rotation is possible for the opposite skyrmion ($Q = -1$). In this case, the rotation direction should be reversed, and the rotation makes the outer magnetization be $+x$. Note that a proper magnetization rotation can cause the same outer magnetization, regardless of the skyrmion charges.

Figure 1(c) shows skyrmions with opposite Q signs in an IMA system. Because of the same outer magnetization, two opposite skyrmions can coexist with the same background outer magnetization. To obtain this magnetization state, we set the insets in Figs. 1(a) and 1(b) as initial states and relax the spin configuration to find a local energy minimum state by a micromagnetic simulation program [23]. We can see that the in-plane skyrmion has a spin structure deformed from the initial states. The spin configuration has a mirror symmetry about the x axis but no symmetry about the y axis. The overall shape of the in-plane skyrmion is a vortex and an antivortex pair. Magnetization rotation and the local deformation of the spin configuration might change the skyrmion charge. With simple vortex descriptions we can verify the in-plane skyrmion charge [24–28]. In magnetic vortex studies, the topological charge of a vortex is $pn/2$, where p is the polarity of the vortex core [p is $+1$ (-1) with a $+z$ $(-z)$ core] and n represents the winding number of the vortex, where n is $+1$ (-1) with a vortex (antivortex). The IMA skyrmion consists of the vortex and antivortex pair, and the polarities of the two cores are opposite. As a result, the sum of topological charges of an IMA skyrmion is ± 1 [Fig. 1(c)].

These vortex and antivortex pairs were often treated as transients [26,29–31] in vortex dynamics. Several studies showed the possibility of existence of stable IMA skyrmion by using skyrmion-bimeron conversions [32], meron pairs in a frustrated magnet [33], and crystal structures [34]. Göbel *et al.* [35] also recently reported that these vortex and antivortex pairs are the skyrmions in IMA. For this, they suggested a special situation: asymmetric arrangements of heavy-metal atoms and disregard of the demagnetization field. However, in this paper, we do not take into account such restrictions for generality and furthermore we show a simple condition for the IMA skyrmion.

IV. STATIC PROPERTIES OF IN-PLANE SKYRMIONS

We now show the detailed shape of skyrmions in an IMA system. In a PMA system, the skyrmion looks like a circular domain. The relaxed magnetization state of a PMA skyrmion with a simplified color code is shown in Fig. 2(a). The different colors show the region where the major magnetization direction is one of $\pm x$, $\pm y$, or $\pm z$. In this PMA skyrmion, the position where $m_z = 0$ is considered to be an edge defining the skyrmion shape [the cyan line in Fig. 2(a)]. By the same description, Fig. 2(b) shows the structure of the relaxed in-plane skyrmion. In this case, the position with $m_x = 0$ is an edge of the in-plane skyrmion. The insets in Fig. 2(b) represent the magnetization configurations on a gray color scale; white corresponds to $m_i = +1$ and black corresponds to $m_i = -1$. The vortex with the $+z$ core is almost symmetric, but the antivortex with the $-z$ core is compressed along the x direction.

This IMA skyrmion is mainly determined by the competition between iDMI and the demagnetization field. To form the skyrmion texture in IMA, perpendicular magnetization is required, but such perpendicular magnetization produces a magnetic charge on the surface of the magnetic material that generates an opposite magnetic field inside the magnet. This is the demagnetization field ($\mathbf{H}_{\text{demag}}$), and its strength is equal to the saturation magnetization (M_S). In an IMA system, the change of the in-plane magnetization in space can produce an effective perpendicular magnetic field because of the iDMI. A simplified magnetization state is shown in the lower inset in Fig. 2(c). When the magnetization is uniform along the x axis and changes from $+y$ to $-y$ on a length scale (l_S) along the y direction, the strength of the iDMI field (H_{DMI}) at the center is $\pi D_{\text{ind}}/(2\mu_0 M_S l_S)$ [36], where D_{ind} is the iDMI energy density and μ_0 is the permeability. Therefore, if $|H_{\text{DMI}}| > M_S$, a perpendicular magnetization can be stabilized in IMA. We know that magnetization change needs exchange length $\sqrt{A/(0.5\mu_0 M_S{}^2)}$, where A is the exchange stiffness constant [27,28]. Inserting the exchange length as l_S results in $M_S < 1.11|D_{\text{ind}}|/\sqrt{\mu_0 A}$.

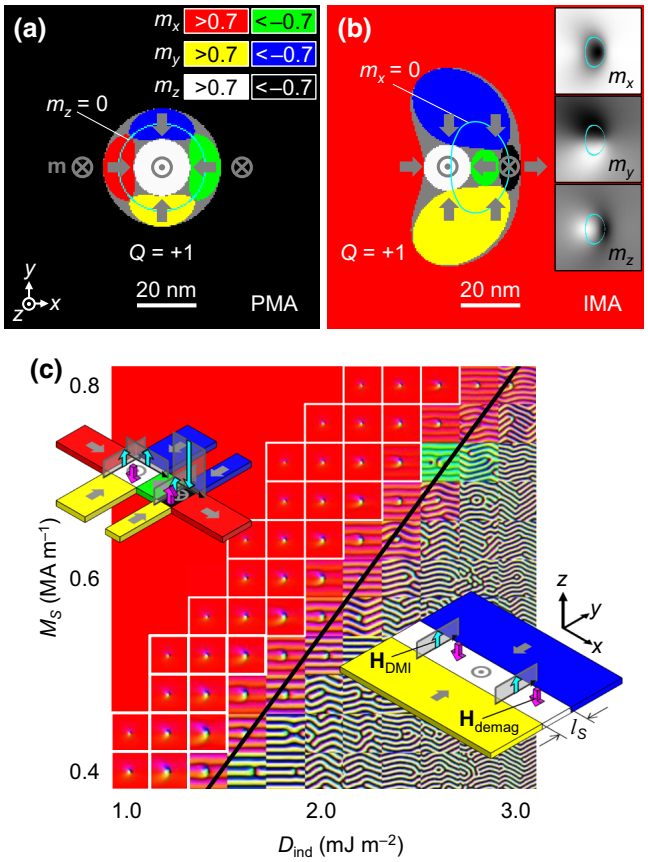

FIG. 2. Skyrmion structure and skyrmion phase diagram. (a) Simplified magnetization structure for a skyrmion in PMA. Colors show the direction ($\pm x, \pm y, \pm z$) of magnetization components that is dominant. The gray arrows depict the magnetization. (b) Simplified magnetization structure for a skyrmion in IMA. The insets show images of m_x, m_y, and m_z components with gray scale (white is +1 and black is –1). (c) Relaxed magnetization states with respect to D_{ind} and M_S. The insets show the simplified magnetic configurations of a skyrmion and a stripe. Purple arrows are the demagnetization field and cyan arrows are the iDMI field. The thick black line is the stripe condition. The parameters are as follows $A = 1.3 \times 10^{-11}$ J m^{-1}, $D_{\text{ind}} = 2.0 \times 10^{-3}$ J m^{-2}, $M_S = 720 \times 10^3$ A m^{-1}, and $t_M = 1$ nm. For (a), we used the PMA energy density ($K_z = 0.6 \times 10^6$ J m^{-3}) to make the perpendicular system. The cell sizes are $0.5 \times 0.5 \times 1$ nm^3 for (a),(b) and $2.5 \times 2.5 \times 1$ nm^3 for (c). Each image size in (c) corresponds to 500×500 nm^2. The periodic boundary condition is used along the x and y axes. We get each magnetization state by relaxation.

The phase diagram of the magnetization states as functions of D_{ind} and M_S is shown in Fig. 2(c). Each magnetization state is obtained by relaxing the initial magnetization state, which contains a single IMA skyrmion in $+x$ outer magnetization such as in Fig. 2(b). Thus, each image represents a local energy minimum state as well as the

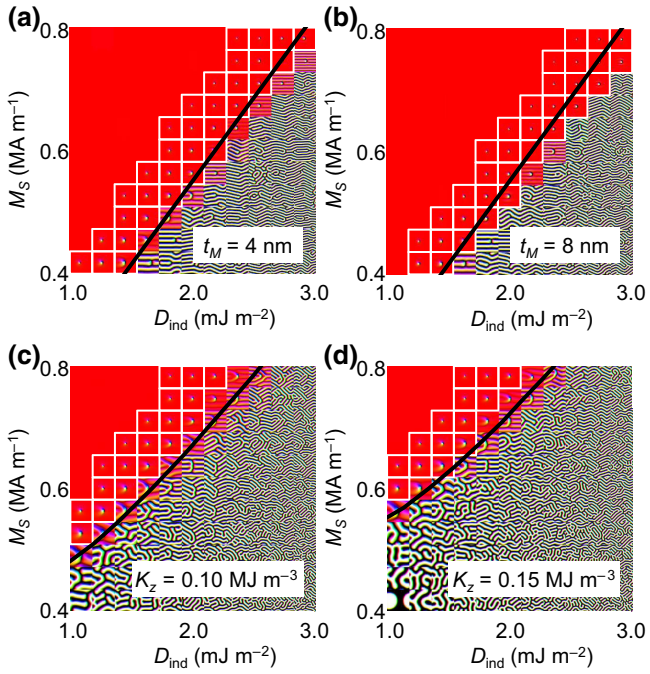

FIG. 3. Relaxed magnetization states with respect to D_{ind} and M_S. The black lines are the generalized stripe condition. The parameters are the same as those used in Fig. 2(c) except for t_M in (a),(b) and K_z in (c),(d).

condition where the IMA skyrmion survives (white boxed images). The black line represents the position where $M_S = 1.11|D_{\text{ind}}|/\sqrt{\mu_0 A}$ (called the "stripe condition"). An increase in D_{ind} or decrease in M_S from this line corresponds to a H_{DMI} value larger than M_S, which produces full stripe domains. This fits well with our expectation because the condition for a stripe domain is derived from a one-dimensional spin structure [the lower inset in Fig. 2(c)]. The stripe condition existing in thin films is noteworthy because it does not rely on the magnetic layer thickness (t_M). So we can see that simulations with different t_M values produce similar results [Figs 3(a) and 3(b)].

An IMA skyrmion can exist near the stripe condition but the required D_{ind} is slightly smaller than that for the stripe condition. The upper inset in Fig. 2(c) depicts a simplified magnetic configuration of the IMA skyrmion. It has $+z$ magnetization stabilized by the perpendicular iDMI field. This iDMI field has an additional contribution because of the magnetization variation from $+x$ to $-x$ along the x direction. Thus, the iDMI field is double that of the stripe states, and therefore the required D_{ind} should be small. At $-z$ magnetization of the IMA skyrmion, m_y variations along the y axis generate the iDMI field assisting $\mathbf{H}_{\text{demag}}$. These two fields make the $-z$ magnetization unstable, and thus these two fields must be compensated by the other iDMI field generated by the m_x variation along the x axis. We know that the iDMI field is inversely proportional to l_S, and thus the area of $-z$ magnetization should have been reduced along the x direction. This is the main origin of the asymmetric shape of the IMA skyrmion.

The discussion so far has confirmed that there is a condition for the presence of an IMA skyrmion. However, it is difficult to implement experimentally because the required DMI is large (approximately 2 mJ m^{-2} or greater). So we explain that an additional PMA energy density (K_z) can solve this problem. K_z generates an effective magnetic field in the $\pm z$ direction and the field strength is $2K_z/(\mu_0 M_S)$. When $2K_z/(\mu_0 M_S)$ exceeds M_S, the system prefers $\pm z$ magnetization and becomes the PMA system. In such a PMA system, the change from $\pm z$ magnetization to $\mp z$ magnetization requires a wall width $\Delta_0 = \sqrt{A/(K_z - 0.5\mu_0 M_S{}^2)}$ [18,19,36]. From this wall width and the exchange length, the modified exchange length of the IMA system with K_z can be expected to be $\sqrt{A/(0.5\mu_0 M_S{}^2 - K_z)}$. We write the generalized stripe condition as follows.

$$\frac{\pi |D_{\text{ind}}|}{2\mu_0 M_S \sqrt{A/(0.5\mu_0 M_S{}^2 - K_z)}} + \frac{2K_z}{\mu_0 M_S} = M_S.$$

The first term on the left-hand side is the iDMI field and the second term is the perpendicular anisotropy field. The right-hand side represents the perpendicular demagnetization field. Figures 3(c) and 3(d) show the results when K_z is added to the simulation in Fig. 2(c). The thick black lines are lines expected for the generalized stripe condition. We can see that additional K_z reduces the required DMI. On the basis of these results, we think that the sample having a spin-reorientation transition (SRT) will be good to observe in-plane skyrmions because the SRT sample shows a PMA-IMA transition [37–39]. IMA near the SRT will have sufficient K_z assisting iDMI.

V. DYNAMIC PROPERTIES OF IN-PLANE SKYRMIONS

Now we apply an electric current to induce the motion of the IMA skyrmion. The electric-current-induced skyrmion motion is an important technical issue in the application area [3,4,11,12]. There are two well-known mechanisms for the motions. One is induced by the current flowing in the magnet, and we call this spin-magnetization-transfer torque (SMT) [3,40–43]. The other comes from the current in the attached heavy-metal layers, and is known as spin-orbit torque (SOT) [3,42,44]. Each effect inherently has a vector property; SMT has the vector **u** representing the current direction and strength, and SOT has the vector **σ** representing a pumped spin direction. Generally, **u** and **σ** are on the x-y plane and can have arbitrary direction; thus, we check the skyrmion velocities as a function of the angle difference between the outer magnetization ($\mathbf{m}_{\text{out}}$) and each of **u** and **σ**. This is a property distinct from the PMA skyrmion because $\mathbf{m}_{\text{out}}$ of the PMA skyrmion is the

$\pm z$ magnetization, which has no angular dependence on **u** and **σ**.

Figure 4 shows the results for the IMA skyrmion velocity in infinite films. We set $\mathbf{m}_{\text{out}}$ as the $-y$ magnetization and change the angle of the SMT effect ($\varphi_{\mathbf{u}}$) and of the SOT effect ($\varphi_{\boldsymbol{\sigma}}$). The red and blue arrows in the lower panel depict skyrmion velocities in the x-y plane. The starting points of these arrows define $\varphi_{\mathbf{u}}$ and $\varphi_{\boldsymbol{\sigma}}$ with respect to $+y$. We can see a weak velocity dependence on $\varphi_{\mathbf{u}}$ but a strong dependence on $\varphi_{\boldsymbol{\sigma}}$. The nonadiabaticity of SMT (β) determines the transverse components of skyrmion velocity with respect to **u** [Fig. 4(a)]. In SOT motion, a larger damping constant (α) increases the transverse speed with respect to $\boldsymbol{\sigma} \times \hat{z}$. Such transverse motion is known as the skyrmion Hall effect [21,22,45]. The velocity results and the skyrmion Hall effect both seem to be quite complicated. However, Thiele's equations are good for predicting the skyrmion velocity (dashed lines and dots), which is useful for describing the motions of well-structured magnetic configurations [3,7,17,41,43,46–50]. The Thiele approach

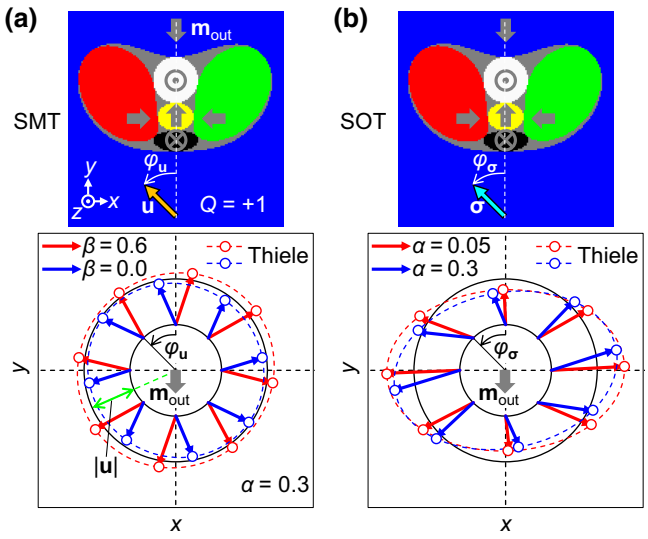

FIG. 4. Skyrmion velocity and spin-torque angle in an infinite film. (a) SMT-driven skyrmion. (b) SOT-driven skyrmion. We set the outer magnetization as $-y$. The upper images show the schematic magnetization state and angle definitions for **u** and **σ**. In the lower images, red and blue arrows represent the velocities of skyrmion motion in the x-y plane. The strengths of SMT and SOT are fixed and only the directions are changed. $\varphi_{\mathbf{u}}$ and $\varphi_{\boldsymbol{\sigma}}$ are the angles. Two concentric black circles depict $|\mathbf{u}|$ as the radius difference. Dashed lines and dots are the expected values from the Thiele approach. The parameters are as follows: $A = 1.3 \times 10^{-11}\,\text{J m}^{-1}$, $D_{\text{ind}} = 1.6 \times 10^{-3}\,\text{J m}^{-2}$, $M_S = 560 \times 10^3\,\text{A m}^{-1}$, $K_z = 0$, $t_M = 1$ nm, and cell size $2.5 \times 2.5 \times 1\,\text{nm}^3$. We use damping constant $\alpha = 0.3$ for (a). To hold the outer magnetization in the $-y$ direction, a small IMA along the y direction ($K_y = 5 \times 10^3\,\text{J m}^{-3}$) is introduced. We set the strength of SMT ($|\mathbf{u}|$) as $5\,\text{m s}^{-1}$ for (a). We use the strength of SOT (τ_d) as 4 mT for (b).

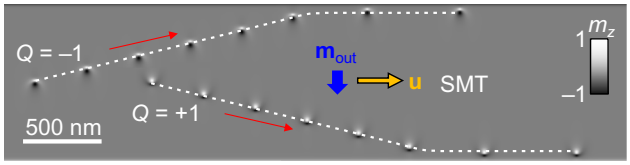

VIDEO 1. SMT-driven skyrmions. Only m_z components are shown with a gray scale (white is +1 and black is −1). Skyrmions are overlapping in a single image with a fixed time step (30 ns) in the static image. The periodic boundary condition is used along the x direction. α is 0.3 and the other parameters are the same as those used in Fig. 4 except for $|\mathbf{u}|$ ($10\,\text{m s}^{-1}$), β (0.6), and τ_d (0).

reveals that the asymmetric shape of the IMA skyrmion is the origin of the complicated skyrmion velocity. This is because gradients of the magnetization state on the x and y axes determine the components of Thiele's equations. (See Appendix A for more details on Thiele's equations).

We show that skyrmions having opposite Q values can move together [51]. Video 1 shows the skyrmion motion in a wire-structured track by SMT and Video 2 shows the motion by SOT. Initially, two IMA skyrmions are placed in a uniform $-y$ magnetization. At the beginning of the motion, opposite Q produces opposite skyrmion Hall effects, but when the skyrmions meet wire edges, the edges generate a repulsive force on the skyrmions [41]. As a result, two skyrmions with opposite Q values can move together along the track direction. We know that the skyrmions act as a data bit, and thus this result means that we can transfer double data bits in a single wire track.

VI. BULK-TYPE DMI AND IN-PLANE SKYRMIONS

Before conclusion of the paper, we briefly show that the same phenomena are possible in the case of bulk-type DMI [3]. The bulk-type DMI prefers a certain chiral spin texture such as $(-z)$-$(+y)$-$(+z)$-$(-y)$-$(-z)$ along the x axis. Figure 5(a) shows a typical form of a skyrmion when the bulk-type DMI is applied to a PMA system. Figure 5(b) shows the form of a skyrmion that may exist in an IMA system. Figure 5(c) shows the material values that IMA

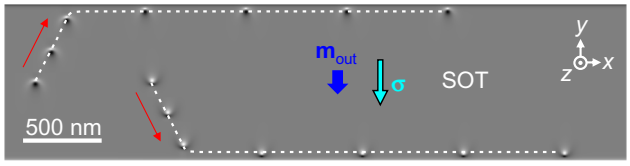

VIDEO 2. SOT-driven skyrmions. Skyrmions are overlapping in a single image with a fixed time step (30 ns) in the static image. The other parameters are the same as those used in Video 1 except for τ_d (8 mT) and $|\mathbf{u}|$ (0).

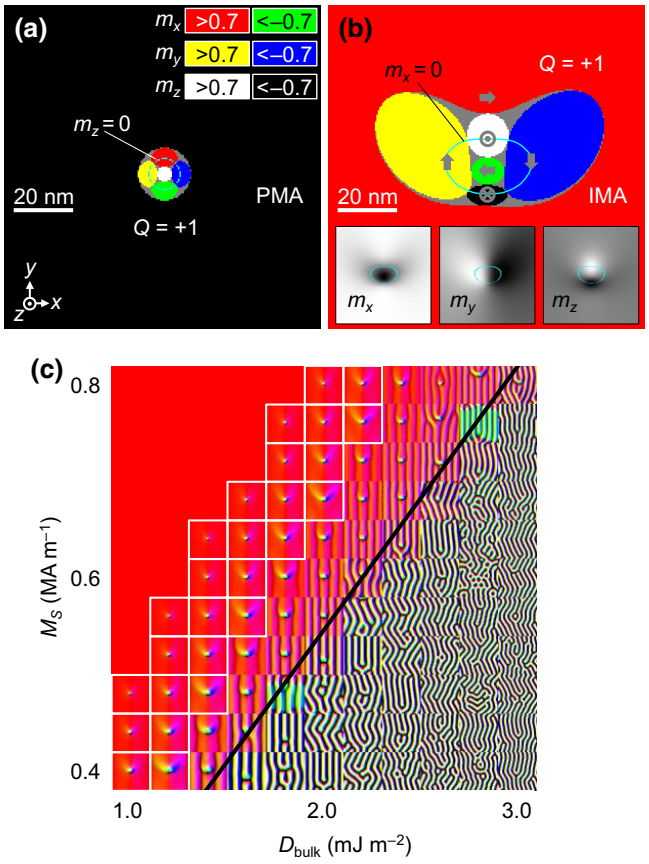

FIG. 5. Skyrmion structure and phase diagram for bulk-type DMI. (a), (b) Simplified skyrmion configurations. (c) Phase diagram and the stripe condition (black line). The parameters are as follows: $A = 1.3 \times 10^{-11}$ J m^{-1}, bulk-DMI energy density $D_{bulk} = 1.6 \times 10^{-3}$ J m^{-2}, $M_S = 680 \times 10^3$ A m^{-1}, and $t_M = 1$ nm. For (a), $K_z = 0.6 \times 10^6$ J m^{-3} to make the perpendicular system. The cell size is $0.5 \times 0.5 \times 1$ nm^3 for (a),(b) and $2.5 \times 2.5 \times 1$ nm^3 for (c). Each image size in (c) corresponds to 500×500 nm^2. The periodic boundary condition) is used along the x and y axes.

skyrmions may have. It is important that such magnetization states are well expected by the same stripe conditions used in the iDMI system.

VII. CONCLUSIONS

In summary, we show the possibility of skyrmion structures in the in-plane-magnetization system using the topological property of the skyrmion, namely, charge conservation under continuous transformation. The in-plane skyrmion can be stabilized by DMI because this interaction can hold the perpendicular magnetization. The important property of this in-plane skyrmion is that skyrmions having opposite charge can coexist in the same outer background magnetization. This is a distinct feature of the in-plane skyrmions over the perpendicular system. This compatibility of opposite skyrmions enables double-bit transfer on a single track. Furthermore, an operator based on these two bits could be possible on a logic gate (the readout head).

ACKNOWLEDGMENTS

This work was supported by the Future Materials Discovery Program through the National Research Foundation of Korea (Grant No. 2015M3D1A1070467) and a National Research Council of Science and Technology grant (Grant No. CAP-16-01-KIST) from the Korean government (MSIP).

APPENDIX A: THIELE'S EQUATIONS

The dynamics of local magnetization are described by the Landau-Lifshitz-Gilbert (LLG) equation as follows:

$$\dot{\mathbf{m}} = -\gamma_0 \mathbf{m} \times \mathbf{H}_{\text{eff}} + \alpha \mathbf{m} \times \dot{\mathbf{m}} - (\mathbf{u} \cdot \nabla)\mathbf{m} + \beta \mathbf{m} \times [(\mathbf{u} \cdot \nabla)\mathbf{m}] + \gamma_0 \tau_d \mathbf{m} \times (\boldsymbol{\sigma} \times \mathbf{m}) + \gamma_0 \tau_f \mathbf{m} \times \boldsymbol{\sigma}, \tag{A1}$$

where $\mathbf{m}$ is the local magnetization, $\dot{\mathbf{m}}$ is the time derivative of $\mathbf{m}$, γ_0 is the gyromagnetic ratio, $\mathbf{H}_{\text{eff}}$ is the effective magnetic field, α is the damping constant, $\mathbf{u}$ represents the SMT effect, β is the nonadiabaticity of SMT, τ_d is the strength of dampinglike SOT, $\boldsymbol{\sigma}$ is the pumped spin direction of SOT, and τ_f is the strength of fieldlike SOT. $\mathbf{H}_{\text{eff}}$ is the sum of the external magnetic field ($\mathbf{H}_{\text{ext}}$) and the internal magnetic field ($\mathbf{H}_{\text{int}}$). The exchange, DMI, dipole, and anisotropy energies generate $\mathbf{H}_{\text{int}}$. In this paper, we set $\mathbf{H}_{\text{ext}} = 0$ and $\tau_f = 0$ because we do not discuss the magnetic field and the fieldlike effects. In addition, we consider only stabilized magnetization states, which means local magnetizations are parallel to $\mathbf{H}_{\text{int}}$. The LLG equation then becomes

$$\dot{\mathbf{m}} = \alpha \mathbf{m} \times \dot{\mathbf{m}} - (\mathbf{u} \cdot \nabla)\mathbf{m} + \beta \mathbf{m} \times [(\mathbf{u} \cdot \nabla)\mathbf{m}] + \gamma_0 \tau_d \mathbf{m} \times (\boldsymbol{\sigma} \times \mathbf{m}). \tag{A2}$$

The Thiele approach is useful when the magnetization configuration is conserved during the motions. This means $\mathbf{m}(x, y) = \mathbf{m}_0(x - V_x t, y - V_y t)$, where V_i is the i-directional speed and t is the time. To get Thiele's equation, we have to convert each torque term in the LLG equation to a speed term by calculating $\int$(LLG equation) $\cdot$ $(\mathbf{m}_0 \times \partial_i \mathbf{m}_0) dx dy$ [3,7,17,41,43,46–49]. Here i is x or y. With use of $\dot{\mathbf{m}} = -V_x \partial_x \mathbf{m}_0 - V_y \partial_y \mathbf{m}_0$ and vector calculus identities, the equations $\mathbf{A} \cdot (\mathbf{B} \times \mathbf{C}) = \mathbf{B} \cdot (\mathbf{C} \times \mathbf{A}) = \mathbf{C} \cdot (\mathbf{A} \times \mathbf{B})$ and $(\mathbf{A} \times \mathbf{B}) \cdot (\mathbf{C} \times \mathbf{D}) = (\mathbf{A} \cdot \mathbf{C})(\mathbf{B} \cdot \mathbf{D}) - (\mathbf{B} \cdot \mathbf{C})(\mathbf{A} \cdot \mathbf{D})$, produce two coupled equations. When only the SMT drives the skyrmion ($\tau_d = 0$), Thiele's equations are

$$-G(u_y - V_y) = D_{xx}(\beta u_x - \alpha V_x), \tag{A3a}$$

$$G(u_x - V_x) = D_{yy}(\beta u_y - \alpha V_y). \tag{A3b}$$

Here $G = -4\pi Q = -\int \mathbf{m}_0 \cdot (\partial_x \mathbf{m}_0 \times \partial_y \mathbf{m}_0) dxdy$, $D_{ij} = \int \partial_i \mathbf{m}_0 \partial_j \mathbf{m}_0 dxdy$, and $\mathbf{u} = (u_x, u_y)$. Equations (A3a) and (A3b) describe the skyrmion velocities in Fig. 4(a). If we consider that only the SOT drives the skyrmion ($\mathbf{u} = 0$), Thiele's equations are

$$GV_y = -\alpha D_{xx} V_x + w_x, \tag{A4a}$$

$$-GV_x = -\alpha D_{yy} V_y + w_y. \tag{A4b}$$

Here w_i $[\gamma_0 \tau_d \int (\boldsymbol{\sigma} \times \mathbf{m}_0) \cdot \partial_i \mathbf{m}_0 dxdy]$ is the speed contribution because of the dampinglike SOT. Equation (A4) well describes the skyrmion motions shown in Fig. 4(b). Note that it is $\partial_x \mathbf{m}_0 \neq \partial_y \mathbf{m}_0$ in the IMA skyrmion that makes the velocity complicated. Inserting $V_y = 0$ in the above equations simply results in $V_x = (\beta/\alpha) u_x$ and $V_x = 1/(\alpha D_{xx}) w_x$. These speed equations are useful to predict the skyrmion speeds in the confined wire structure as shown in Videos 1 and 2.

[1] V. K. Joshi, Spintronics: A contemporary review of emerging electronics devices, Eng. Sci. Technol. an Int. J. **19**, 1503 (2016).

[2] J. Åkerman, Toward a universal memory, Science **308**, 508 (2005).

[3] R. Tomasello, E. Martinez, R. Zivieri, L. Torres, M. Carpentieri, and G. Finocchio, A strategy for the design of skyrmion racetrack memories, Sci. Rep. **4**, 6784 (2014).

[4] J. Sampaio, V. Cros, S. Rohart, A. Thiaville, and A. Fert, Nucleation, stability and current-induced motion of isolated magnetic skyrmions in nanostructures, Nat. Nanotechnol. **8**, 839 (2013).

[5] K.-W. Moon, D.-H. Kim, S.-C. Yoo, S.-G. Je, B. S. Chun, W. Kim, B.-C. Min, C. Hwang, and S.-B. Choe, Magnetic bubblecade memory based on chiral domain walls, Sci. Rep. **5**, 9166 (2015).

[6] N. Romming, C. Hanneken, M. Menzel, J. E. Bickel, B. Wolter, K. Von Bergmann, A. Kubetzka, and R. Wiesendanger, Writing and deleting single magnetic skyrmions, Science **341**, 636 (2013).

[7] N. Nagaosa and Y. Tokura, Topological properties and dynamics of magnetic skyrmions, Nat. Nanotechnol. **8**, 899 (2013).

[8] A. De Lucia, K. Litzius, B. Krüger, O. A. Tretiakov, and M. Kläui, Multiscale simulations of topological transformations in magnetic-skyrmion spin structures, Phys. Rev. B **96**, 020405(R) (2017).

[9] X. Z. Yu, N. Kanazawa, Y. Onose, K. Kimoto, W. Z. Zhang, S. Ishiwata, Y. Matsui, and Y. Tokura, Near room-temperature formation of a skyrmion crystal in thin-films of the helimagnet FeGe, Nat. Mater. **10**, 106 (2011).

[10] A. Fert, N. Reyren, and V. Cros, Magnetic skyrmions: Advances in physics and potential applications, Nat. Rev. Mater. **2**, 17031 (2017).

[11] G. Finocchio, F. Büttner, R. Tomasello, M. Carpentieri, and M. Kläui, Magnetic skyrmions: From fundamental to applications, J. Phys. D. Appl. Phys. **49**, 423001 (2016).

[12] J. Iwasaki, M. Mochizuki, and N. Nagaosa, Current-induced skyrmion dynamics in constricted geometries, Nat. Nanotechnol. **8**, 742 (2013).

[13] J. Li, A. Tan, K. W. Moon, A. Doran, M. A. Marcus, A. T. Young, E. Arenholz, S. Ma, R. F. Yang, C. Hwang, and Z. Q. Qiu, Imprinting antivortex states from ferromagnetic Fe into antiferromagnetic NiO in epitaxial NiO/Fe/Ag(001) microstructures, Nat. Commun. **5**, 4704 (2014).

[14] L. Kong and J. Zang, Dynamics of an Insulating Skyrmion Under a Temperature Gradient, Phys. Rev. Lett. **111**, 067203 (2013).

[15] T. Moriya, Anisotropic superexchange interaction and weak ferromagnetism, Phys. Rev. **120**, 91 (1960).

[16] I. Dzyaloshinsky, A thermodynamic theory of "weak" ferromagnetism of antiferromagnetics, J. Phys. Chem. Solids **4**, 241 (1958).

[17] K. W. Kim, K. W. Moon, N. Kerber, J. Nothhelfer, and K. Everschor-Sitte, Asymmetric skyrmion Hall effect in systems with a hybrid Dzyaloshinskii-Moriya interaction, Phys. Rev. B **97**, 224427 (2018).

[18] S. G. Je, D. H. Kim, S. C. Yoo, B. C. Min, K. J. Lee, and S. B. Choe, Asymmetric magnetic domain-wall motion by the Dzyaloshinskii-Moriya interaction, Phys. Rev. B **88**, 214401 (2013).

[19] A. Hrabec, N. A. Porter, A. Wells, M. J. Benitez, G. Burnell, S. McVitie, D. McGrouther, T. A. Moore, and C. H. Marrows, DMI meter: Measuring the Dzyaloshinskii-Moriya interaction inversion in Pt/Co/Ir/Pt multilayers, Phys. Rev. B **90**, 020402 (2014).

[20] A. Ebrahim and M. Savci, Derivation of the skyrme lagrangian, Phys. Lett. B **171**, 429 (1986).

[21] X. Zhang, Y. Zhou, and M. Ezawa, Magnetic bilayer-skyrmions without skyrmion hall effect, Nat. Commun. **7**, 10293 (2016).

[22] W. Jiang, X. Zhang, G. Yu, W. Zhang, X. Wang, M. Benjamin Jungfleisch, J. E. Pearson, X. Cheng, O. Heinonen, K. L. Wang, Y. Zhou, A. Hoffmann, and S. G. E. Te Velthuis, Direct observation of the skyrmion hall effect, Nat. Phys. **13**, 162 (2017).

[23] A. Vansteenkiste, J. Leliaert, M. Dvornik, M. Helsen, F. Garcia-Sanchez, and B. Van Waeyenberge, The design and verification of MuMax3, AIP Adv. **4**, 107133 (2014).

[24] C. L. Chien, F. Q. Zhu, and J. G. Zhu, Patterned nanomagnets, Phys. Today **60**, 40 (2007).

[25] Z. M. Dai, Y. Y. Dai, W. Liu, T. T. Wang, X. T. Zhao, X. G. Zhao, and Z. D. Zhang, Magnetization reversal of vortex states driven by out-of-plane field in the nanocomposite Co/Pd/Ru/Py disks, Appl. Phys. Lett. **111**, 022404 (2017).

[26] B. Van Waeyenberge, A. Puzic, H. Stoll, K. W. Chou, T. Tyliszczak, R. Hertel, M. Fähnle, H. Brückl, K. Rott, G. Reiss, I. Neudecker, D. Weiss, C. H. Back, and G. Schütz, Magnetic vortex core reversal by excitation with short bursts of an alternating field, Nature **444**, 461 (2006).

[27] R. Hertel and C. M. Schneider, Exchange Explosions: Magnetization Dynamics During Vortex-Antivortex Annihilation, Phys. Rev. Lett. **97**, 177202 (2006).

[28] O. A. Tretiakov and O. Tchernyshyov, Vortices in thin ferromagnetic films and the skyrmion number, Phys. Rev. B **75**, 012408 (2007).

[29] R. M. Otxoa, S. Petit-Watelot, M. Manfrini, I. P. Radu, A. Thean, J.-V. Kim, and T. Devolder, Dynamical influence

of vortex-antivortex pairs in magnetic vortex oscillators, J. Magn. Magn. Mater. **394**, 292 (2015).
[30] K. S. Lee, B. W. Kang, Y. S. Yu, and S. K. Kim, Vortex-antivortex pair driven magnetization dynamics studied by micromagnetic simulations, Appl. Phys. Lett. **85**, 1568 (2004).
[31] S. K. Kim, Y. S. Choi, K. S. Lee, K. Y. Guslienko, and D. E. Jeong, Electric-current-driven vortex-core reversal in soft magnetic nanodots, Appl. Phys. Lett. **91**, 082506 (2007).
[32] X. Zhang, M. Ezawa, and Y. Zhou, Magnetic skyrmion logic gates: Conversion, duplication and merging of skyrmions, Sci. Rep. **5**, 9400 (2015).
[33] Y. A. Kharkov, O. P. Sushkov, and M. Mostovoy, Bound States of Skyrmions and Merons Near the Lifshitz Point, Phys. Rev. Lett. **119**, 207201 (2017).
[34] X. Z. Yu, W. Koshibae, Y. Tokunaga, K. Shibata, Y. Taguchi, N. Nagaosa, and Y. Tokura, Transformation between meron and skyrmion topological spin textures in a chiral magnet, Nature **564**, 95 (2018).
[35] B. Göbel, A. Mook, J. Henk, I. Mertig, and O. A. Tretiakov, Magnetic bimerons as skyrmion analogues in in-plane magnets, Phys. Rev. B **99**, 060407 (2019).
[36] A. Thiaville, S. Rohart, É. Jué, V. Cros, and A. Fert, Dynamics of dzyaloshinskii domain walls in ultrathin magnetic films, Europhys. Lett. **100**, 57002 (2012).
[37] Y. Z. Wu, C. Won, A. Scholl, A. Doran, H. W. Zhao, X. F. Jin, and Z. Q. Qiu, Magnetic Stripe Domains in Coupled Magnetic Sandwiches, Phys. Rev. Lett. **93**, 117205 (2004).
[38] J. Choi, J. Wu, C. Won, Y. Z. Wu, A. Scholl, A. Doran, T. Owens, and Z. Q. Qiu, Magnetic Bubble Domain Phase at the Spin Reorientation Transition of Ultrathin Fe/Ni/Cu(001) Film, Phys. Rev. Lett. **98**, 207205 (2007).
[39] C. Won, Y. Z. Wu, J. Choi, W. Kim, A. Scholl, A. Doran, T. Owens, J. Wu, X. F. Jin, H. W. Zhao, and Z. Q. Qiu, Magnetic stripe melting at the spin reorientation transition in Fe Ni Cu(001), Phys. Rev. B **71**, 224429 (2005).
[40] A. Thiaville, Y. Nakatani, J. Miltat, and Y. Suzuki, Micromagnetic understanding of current-driven domain wall motion in patterned nanowires, Europhys. Lett. **69**, 990 (2005).
[41] J. Iwasaki, M. Mochizuki, and N. Nagaosa, Universal current-velocity relation of skyrmion motion in chiral magnets, Nat. Commun. **4**, 1463 (2013).
[42] K. Moon, C. Kim, J. Yoon, J. W. Choi, D. Kim, K. M. Song, D. Kim, B. S. Chun, and C. Hwang, A spin torque meter with magnetic facet domains, Nat. Commun. **9**, 3788 (2018).
[43] J. Iwasaki, W. Koshibae, and N. Nagaosa, Colossal spin transfer torque effect on skyrmion along the edge, Nano Lett. **14**, 4432 (2014).
[44] K.-S. Ryu, L. Thomas, S.-H. Yang, and S. Parkin, Chiral spin torque at magnetic domain walls, Nat. Nanotechnol. **8**, 527 (2013).
[45] K. Litzius, I. Lemesh, B. Krüger, P. Bassirian, L. Caretta, K. Richter, F. Büttner, K. Sato, O. A. Tretiakov, J. Förster, R. M. Reeve, M. Weigand, I. Bykova, H. Stoll, G. Schütz, G. S. D. Beach, and M. Klaüi, Skyrmion hall effect revealed by direct time-resolved X-ray microscopy, Nat. Phys. **13**, 170 (2017).
[46] A. A. Thiele, Steady-state Motion of Magnetic Domains, Phys. Rev. Lett. **30**, 230 (1973).
[47] O. A. Tretiakov, D. Clarke, G. W. Chern, Y. B. Bazaliy, and O. Tchernyshyov, Dynamics of Domain Walls in Magnetic Nanostrips, Phys. Rev. Lett. **100**, 127204 (2008).
[48] D. J. Clarke, O. A. Tretiakov, G. W. Chern, Y. B. Bazaliy, and O. Tchernyshyov, Dynamics of a vortex domain wall in a magnetic nanostrip: Application of the collective-coordinate approach, Phys. Rev. B **78**, 134412 (2008).
[49] I. A. Ado, O. A. Tretiakov, and M. Titov, Microscopic theory of spin-orbit torques in two dimensions, Phys. Rev. B **95**, 094401 (2017).
[50] S. K. Kim, Dynamics of bimeron skyrmions in easy-plane magnets induced by a spin supercurrent, Phys. Rev. B **99**, 224406 (2019).
[51] J. Barker and O. A. Tretiakov, Static and Dynamical Properties of Antiferromagnetic Skyrmions in the Presence of Applied Current and Temperature, Phys. Rev. Lett. **116**, 147203 (2016).